

The influence of exact exchange corrections in van der Waals layered narrow bandgap black phosphorus

Ø Prytz and E Flage-Larsen

Department of Physics, University of Oslo, PO Box 1048, Blindern, NO-0316 Oslo, Norway

E-mail: oystein.prytz@fys.uio.no

Received 10 August 2009, in final form 2 October 2009

Published 8 December 2009

Online at stacks.iop.org/JPhysCM/22/015502

Abstract

We study the electronic structure of black phosphorus by combining state-of-the-art density functional theory, multiple scattering calculations and electron energy loss spectroscopy. The hybrid functionals HSE03 and PBE0 are tested to investigate whether they give an improved description compared to the more traditional PZ-LDA and PBE-GGA functionals. These calculations are compared with investigations of the conduction band using electron energy loss spectroscopy and calculations based on the real-space multiple scattering approach, and previous determinations of the bandgap. The hybrid functional HSE03 gives an improved correspondence with these experiments. Comparisons of the calculated valence band with previous XPS studies yield acceptable agreement for the traditional functionals, while the results from the hybrid functionals are less satisfactory, since the hybrid functionals overestimate the valence band width significantly.

1. Introduction

The success of the modern implementations of density functional theory (DFT) [1, 2] is indisputable. However, even though the Kohn–Sham (KS) equations [2] are in principle able to provide the exact ground state, significant approximations are needed to ensure feasible extended-system calculations. These approximations govern the exchange–correlation energy beyond the Hartree level [3]. Two of the most used classes of functionals are those that rely on the local density approximation (LDA) [1] and the semi-local generalized gradient approximation (GGA) [4–7]. Two major problems exist with the traditional LDA and GGA functionals: their local form and the delocalization error due to the lack of exact exchange. The various DFT functionals are discussed in numerous excellent articles [8–10, 3].

Another subtlety is related to the KS formalism where pseudostates are introduced. There is no formal justification for identifying these with true single-particle states. Despite this, comparisons with experimental spectra often yield surprisingly good agreement. For a more consistent treatment it is necessary to go beyond the KS formalism to, for example, quasi-particle approaches such as the GW approximation [11].

The most stable form of phosphorus at ambient temperature and pressure is the orthorhombic modification, often called black phosphorus to distinguish it from other forms which are red or white in colour. The crystal structure of black phosphorus is made up of puckered layers of atoms stacked along the crystallographic b axis [12, 13], see figure 1. While each atom is covalently bonded to three neighbours in the same layer, the interaction between the layers is mainly van der Waals like [14, 15]. Such forces are exceedingly difficult to calculate *ab initio*, even for simple molecules. There exist methodologies to properly treat van der Waals forces [16], but due to their intricate nature with both attractive and repulsive long-range correlation components it is difficult to compose a general model that accounts for all the effects in extended systems. Even though the traditional LDA and GGA functionals do not incorporate long-range correlation interactions, they sometimes give the impression of a van der Waals interaction due to an exchange residue [17].

A new breed of functionals has been developed [18–20] to include a fixed portion of the Fock exchange, while treating the correlation effects at the DFT level. In these so-called hybrid functionals, the delocalization error is partly corrected, and for the full-range hybrid functionals the exchange residue should also be partly removed. The success of these functionals was

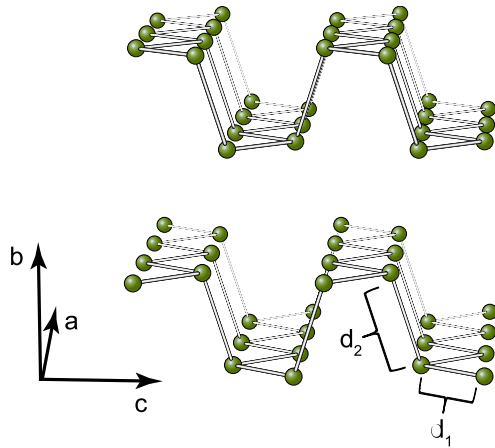


Figure 1. The crystal structure of black phosphorus is composed of puckered layers stacked along the b axis. The interlayer interaction is mainly through van der Waals forces. The intralayer bonding distances d_1 and d_2 are indicated.

immediate in the description of molecular systems, yielding in some cases close to chemical accuracy [21–23]. However, widespread application of these functionals in solids has been limited due to computational costs and problematic boundary conditions. It should also be noted that an exact treatment of the exchange is not expected to fully cure the erroneous behaviour of the traditional local functionals. For this, a more proper treatment of the long-range correlation effects is also needed, which is especially important for systems with known van der Waals interactions. While such functionals exist [24], they have so far only been tested on simple molecular systems. Still, functionals which incorporate a portion of Fock exchange show significant corrections (bandgaps and structural properties) over the traditional functionals for many benchmark solids [25]. For systems incorporating a mixture of covalent bonds and van der Waals interactions such functionals may yield important corrections.

In the following, we investigate the electronic structure of black phosphorus, where both covalent and van der Waals bonding play a central role. The density of states above the Fermi level is studied using a combination of electron energy loss spectroscopy (EELS) [26] and real-space multiple scattering (RSMS) calculations [27]. These calculations utilize self-consistent potentials in a purely local formalism. We go on to perform DFT calculations of the electronic structure using the traditional PZ-LDA [28] and PBE-GGA [29] functionals, and the HSE03 [18] and PBE0 [19] functionals which include Fock corrections. The results of these calculations are compared to illustrate the effect of including the Fock terms. Furthermore, we compare our results to previous work on the valence band using x-ray photoelectron spectroscopy (XPS) [30] and investigations of the bandgap [31, 14].

2. Methodology

2.1. Sample synthesis and preparation

Crystals of black phosphorus were prepared according to the route described by Lange *et al* [32]. The starting materials

were red phosphorus (Aldrich, 99.999%), gold (L. Light, 99.9995%, powder), tin (Merck, p.a.) and tin(IV) iodide (Aldrich, 99.999%, anhydrous). These materials were weighed out in molar proportions 14:1:1:0.047 and heated for 12 days at 650 °C in an evacuated and sealed silica glass ampoule. Slow cooling to room temperature gave up to 1 mm sized crystals in the shape of needles and plates. Powder x-ray diffraction was used to verify that the crystals were black phosphorus.

In order to avoid excessive reaction with oxygen or water in the atmosphere, the samples for TEM were prepared immediately before each experimental session. Single crystals of phosphorus were crushed in ethanol and deposited on a carbon film suspended on a copper grid. The samples were then inserted into the microscope as soon as possible. Ductile deformation of the crystals was observed upon crushing, although enough fine particles were produced to perform the EELS investigations. Large flakes of the material were sometimes seen and we expected a preferential orientation of the particles on the TEM grid.

2.2. Electron energy loss spectroscopy

In EELS, we measure the energy loss suffered by an incident electron due to interactions with a sample. While there are many excitation processes that may cause energy loss, the most important for the investigation of condensed matter are the plasmon and single-electron excitations. In the latter, a single electron in the initial state $|\Psi_i\rangle$ absorbs energy from the incident electron and is excited into an empty state $|\Psi_f\rangle$ above the Fermi level, thus probing the conduction band of the material. The observed scattering cross section σ at an energy loss E can be described in the single-electron approximation using the Fermi golden rule [26, 33]:

$$\frac{d^2\sigma(E, \mathbf{q})}{dE d\mathbf{q}} = \frac{4\gamma^2}{a_0^2 \mathbf{q}^4} \rho(E_i + E) |\langle \Psi_f | e^{i\mathbf{q}\cdot\mathbf{r}} | \Psi_i \rangle|^2. \quad (1)$$

Here \mathbf{q} is the scattering vector determined by the experimental set-up, \mathbf{r} is the position of the scattering event, a_0 is the Bohr radius, γ is the relativistic correction factor and E_i is the energy of the electron in the initial state. The difference in the energy of the final and initial states $E_f - E_i$ equals the energy loss E of the incident electron and $\rho(E_i + E)$ is the density of empty states (conduction DOS). For small chosen values of \mathbf{q} the dipole approximation is valid, in which case the EELS experiment probes the atom-specific symmetry projected DOS above the Fermi level [26].

In the present work, we have investigated the L_2 and L_3 edges of phosphorus, which are due to excitations into the conduction band of the $2p_{1/2}$ and $2p_{3/2}$ electrons, respectively. The EELS experiments were performed using a JEOL 2010F transmission electron microscope operated at 197 kV and fitted with a Gatan GIF200 imaging filter. Due to previous experience with red phosphorus evaporating under the electron beam, the experiments were performed at 77 K using a specimen holder for liquid nitrogen. The composition of the samples was checked using energy-dispersive x-ray analysis, which sometimes yielded small amounts of oxygen (<3 at.%) in addition to phosphorus. These particles were avoided.

The absence of oxygen in the particles studied was also verified by the absence of the oxygen K edge in the EELS spectra. Electron diffraction and imaging revealed flakes of material of almost uniform thickness, mostly oriented with the crystallographic [010] direction perpendicular to the particle surface. Selected-area diffraction patterns were obtained and indexed, giving lattice parameters in good agreement with previous work [12].

The EELS experiments were performed with the microscope in imaging mode, at an energy resolution of approximately 1.2 eV as measured by the full width at half-maximum of the zero loss peak. A spectrometer dispersion of 0.2 eV/channel was used. Thickness effects were removed from the core loss spectra using the Fourier ratio method implemented in the Gatan EELS analysis extension to Digital Micrograph.

2.3. Computational approaches

2.3.1. Real-space multiple scattering calculations. Electron energy loss spectra were calculated using the real-space multiple scattering code FEFF8 [27]. In these calculations, self-consistent muffin-tin potentials ($R_{\text{MT}} = 0.677 \text{ \AA}$) were obtained for a spherical cluster of 116 atoms using Hedin–Lundqvist (LDA) self-energies [34]. While clusters containing up to 700 atoms were tested for the full multiple scattering (FMS) calculations, all the main spectral features were reproduced for clusters as small as 150 atoms. The spectra presented here were all calculated for 179 atoms in the FMS cluster, while for the density-of-states calculations a cluster of 358 atoms was used. Three different approaches implemented in the FEFF8 code were used to account for the introduction of a core hole by the excitation process: (a) no core hole, the potential and final states are those of the ground state; (b) the final states and the potential are found self-consistently in the presence of a fully screened core hole and (c) dynamic screening of the core-hole photoelectron interaction [35]. While the Fermi-level and final-state energies are found in the self-consistent field calculations, FEFF8 has no means of determining the initial-state binding energies, apart from assuming that they are equal to the free-atom values. Therefore, the calculated spectra were aligned in energy to the experimental spectra.

2.3.2. Density functional theory. DFT calculations were based on Perdew–Zunger parametrization [28] in the LDA (PZ-LDA), Perdew–Burke–Ernzerhof [29] in the GGA (PBE-GGA), Heyd–Scuseria–Ernzerhof (HSE03) [18] and the modified Perdew–Burke–Ernzerhof (PBE0) [19] exchange–correlation functionals. Both hybrid functionals (HSE03 and PBE0) were evaluated within the GGA. The projector-augmented-wave (PAW) [36, 37] method was employed. All calculations were done using a version of the Vienna *ab initio* simulation package (VASP) [37–42] where the hybrid functionals have been implemented.

An energy cutoff of 450 eV and a Γ -centred k -point grid of $10 \times 4 \times 8$ were necessary to obtain convergence of the total energy to within 2 meV.

The hybrid functionals include a portion of Hartree–Fock exchange and evaluate the remainder exchange from the base functional used. In this work we employ HSE03 and PBE0 hybrid functionals, which both include a quarter of the Hartree–Fock exchange. The concept of the quarter mixing ratio is based on work done by Ernzerhof and co-workers [43–45]. More formally, the exchange–correlation energy for the PBE0 functional is defined as

$$E_{\text{xc}}^{\text{PBE0}} = \frac{1}{4}E_{\text{x}}^{\text{HF}} + \frac{3}{4}E_{\text{x}}^{\text{PBE}} + E_{\text{c}}^{\text{PBE}}, \quad (2)$$

where the subscript indicates exchange (x) or correlation (c) energy. The superscripts signal how to evaluate the given energy, where HF is Hartree–Fock exchange and PBE is exchange and correlation from the PBE functional. The HSE03 functional is based on a range-separated PBE0 functional as follows:

$$E_{\text{xc}}^{\text{HSE03}} = \frac{1}{4}E_{\text{x}}^{\text{HF,sr}} + \frac{3}{4}E_{\text{x}}^{\text{PBE,sr}} + E_{\text{x}}^{\text{PBE,lr}} + E_{\text{c}}^{\text{PBE}}, \quad (3)$$

where sr and lr terms are the short and long ranged parts of the exchange energy. This range separation is defined by dividing the Coulomb kernel such that

$$\frac{1}{r} = \frac{\text{erfc}(\mu r)}{r} + \frac{\text{erf}(\mu r)}{r}, \quad (4)$$

where the first and second terms describe the short- and long-range part of the kernel. The parameter μ determines the range separation. For the HSE03 functional the range separation is $\mu = 0.3 \text{ \AA}^{-1}$. The range separation is motivated from two considerations: first, it allows the calculation of the exact exchange on a coarser grid, thus improving convergence, and, second, it gives the possibility of investigating the range dependence of the exact exchange energy.

Structural relaxation was performed using the residual minimization scheme, direct inversion in the iterative subspace (RMM-DIIS) [46] algorithm, with a force cutoff of 0.01 eV \AA^{-1} . However, as will be seen, the relaxation does not yield satisfactory results and in the remainder of this paper experimental structure parameters [12] are used for consistency.

3. Results and discussion

3.1. Structure relaxation

The experimental lattice parameters and atomic positions of Cartz *et al* [12] were used as a starting point for the relaxation. The resulting lattice parameters and atomic positions are given in table 1, while bond lengths and bond angles are given in table 2.

A 1% and –5% error is observed in the b and c axes with the PZ-LDA functional, while the a axis remains similar to the experimental result. The PBE-GGA functional performs marginally better than the PZ-LDA for the a and c axes, which is reflected in the covalent d_1 and d_2 bond lengths. However, the interlayer van der Waals distance is overestimated by about 15%. For both the PZ-LDA and PBE-GGA functionals, the long-range exchange residue [17]

Table 1. The relaxed cell parameters and positions found using the PZ-LDA, PBE-GGA and HSE03 functionals, compared to the experimental values of Cartz *et al* [12].

Functional	a (Å)	b (Å)	c (Å)	y	z
PZ-LDA	3.3102	10.5510	4.1308	0.1064	0.0710
PBE-GGA	3.3071	11.2686	4.5547	0.0990	0.0866
HSE03	3.2841	11.1352	4.5268	0.0937	0.0879
PBE0	Not converged	—	—	—	—
Exp.	3.3133(9)	10.473(5)	4.374(2)	0.1034(7)	0.0806(12)

Table 2. The relaxed bond distances and angles found using the PZ-LDA, PBE-GGA and HSE03 functionals, compared to the experimental values of Cartz *et al* [12]. d_1 and d_2 refers to the intralayer bonding distances indicated in figure 1, while vdW is the interlayer van der Waals distance.

Functional	vdW (Å)	d_1 (Å)	d_2 (Å)	α_1 (deg)	α_2 (deg)
PZ-LDA	2.9052	2.2197	2.2446	96.4294	100.0256
PBE-GGA	3.5157	2.2250	2.2606	96.0071	103.4985
HSE03	3.4805	2.2023	2.2338	96.4210	103.7326
PBE0	Not converged	—	—	—	—
Exp.	3.0707	2.2227	2.2777	96.3730	101.9106

gives rise to an artificial interlayer bonding that mimics the van der Waals interaction. For PBE-GGA this potential minimum occurs at a larger distance than for PZ-LDA, yielding a significant overestimation of the interlayer bonding distance. The exchange residue needs to be corrected before applying long-range correlation corrections through, for example, Møller–Plesset (MP2)-like perturbations [24].

The HSE03 functional does not correct the exchange residue in the PBE-GGA functional due to the lack of long-range exact exchange. Corrections are expected in the semi-local region, mainly due to delocalization corrections. Indeed, a slight contraction is observed in the covalent bond lengths d_1 and d_2 due to these corrections, but only minor corrections are observed for the van der Waals layer distance.

The PBE0 functional contains long-range exact exchange and should be able to partially correct the exchange residue which gives the fictitious van der Waals bonding observed with the PZ-LDA, PBE-GGA and HSE03 functionals. Thus, we were not able to converge the structure with the PBE0 functional within the force cutoff limits used for the other functionals. This lack of convergence for the PBE0 functional is a strong indication of a successful partial correction of the long-range residual exchange present in the PBE functional, as was suggested in a previous study [47]. Due to the multi-dimensional force and energy relaxation problem, a manual relaxation of the isolated interlayer purely based on a minimization of the energy is not included. Any inherent residual forces would likely not fully reflect the reality of the functional’s deficiencies.

The results from the relaxations clearly show the deficiency of the current functionals. The mixture of covalent and van der Waals bonds are very difficult to describe, and currently there are no feasible methods to fully remedy these problems for extended systems. Hence, throughout the rest of this work, we will exclusively use the experimental structural parameters [12].

3.2. Comparisons of the experimental and theoretical conduction band

Figure 2 shows the experimental L edges of phosphorus together with the RSMS calculations. At about 130 eV energy loss we observe features associated with the excitation of 2p electrons into empty states of s and d character (the L_2 and L_3 edges). At somewhat higher energy losses (about 190 eV) we also observe energy loss features resulting from the excitations of the 2s electrons.

The spectra in figure 2(a) are aligned and normalized to the initial peak. The modelled spectra closely follow the observed intensity up to about 140 eV, after which the discrepancies are larger. All the models overestimate the intensity in the region from about 140 to 160 eV, while for the spectrum as a whole, the model without a core hole is the most successful in terms of the overall relative intensity. The calculated intensity close to the edge onset is sensitive to the treatment of the core hole [27]. The differences in relative intensity seen in figure 2(a) may therefore indicate that the core-hole treatment is not fully successful.

Figure 2(b) shows a close-up of the near-edge region of the $L_{2,3}$ edge, scaled to enhance the fine structure of the edge. Several features (marked A–E) are readily identified in the experimental spectrum, all of which are also apparent in the modelled spectra. While the model without a core hole seems more successful in reproducing the relative intensities, the two models that include a core hole in the potential are clearly better at reproducing the features close to the edge onset. However, the features’ position in energy is not well described in any of the models. The spectra in figure 2(b) are aligned to the initial peak (A), clearly showing that the correspondence in energy becomes progressively worse when moving away from the edge onset. At the feature E, the discrepancy is more than 4 eV. Similar deviations of RSMS calculated spectra from experimental observations were reported for the carbon K edge of graphite and attributed to a failure of the muffin-tin approximation used [48]. As with this previous study our RSMS calculations rely on the muffin-tin approximation, which often yields good results for close-packed systems. However, discrepancies should be expected for systems where the atomic spheres give poor volume filling and where the assumption of spherical symmetry breaks down. Thus, both graphite and black phosphorus are systems where we should expect the muffin-tin approximation to break down. In comparison, the observed discrepancies between experiments and RSMS calculations are significantly larger than what has been reported for the phosphorus L edge in, for example, CoP_3 and NiP_3 [49, 50]. Although these materials

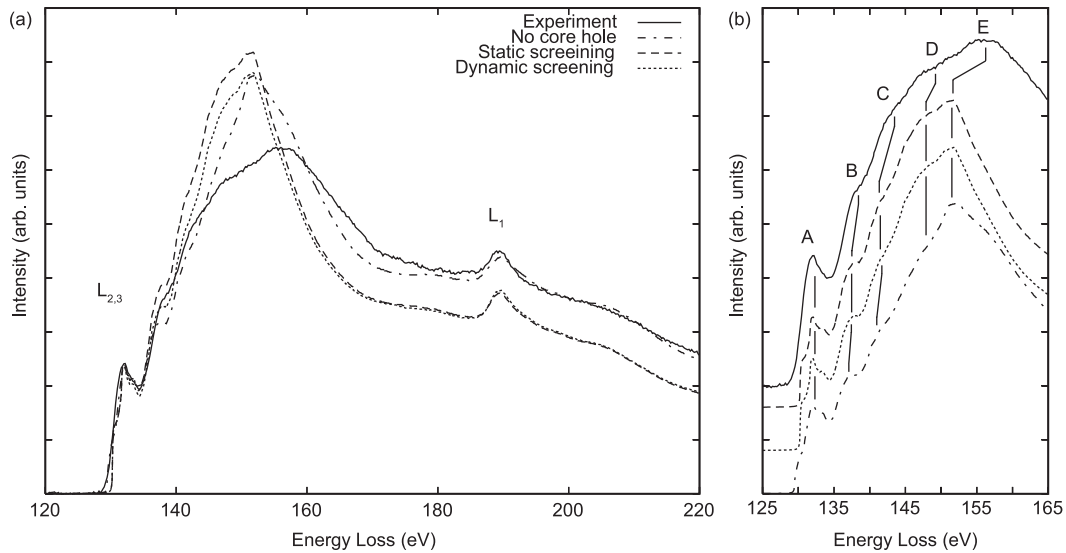


Figure 2. (a) The experimental L edges of phosphorus together with calculated RSMS spectra using different core-hole screening schemes. (b) Close-up of the $L_{2,3}$ near-edge region showing the fine structure in both the experimental and theoretical spectra.

cannot be considered close-packed, they are significantly less open than black phosphorus, and both the edge features and their position in energy are accurately predicted by RSMS calculations. Furthermore, for a correct description of van der Waals interaction, both long-range exchange and correlation effects must be handled properly. Thus, it should not be expected that the combination of local and spherical muffin-tin potentials as employed by FEFF8 should be able to accurately account for the electronic structure in this material. This is confirmed by our comparisons of calculated spectra and the DOS with experiments.

While the RSMS calculations do not give the correct position in energy, the presence of all significant features is accounted for. In the dipole limit, these features can be traced back to the s- and d-DOS of the excited phosphorus atom. Figure 3 shows this density of states calculated by FEFF8 in the presence of a core hole in the 2p shell. Peaks in the DOS are labelled according to their most likely correspondence with features of the experimental and modelled spectra. From this, it is clear that the fine structure of the $L_{2,3}$ edges is dominated by transitions to empty states of d character, but with a significant s-d hybridization in the case of peak A. The experiments show that the DOS calculated with the RSMS approach is concentrated too close to the Fermi level such that a significantly increased dispersion is needed to obtain better agreement with the experiments.

To move beyond the approximations made in the RSMS calculations, we calculated the density of states within the DFT framework, comparing both traditional (PZ-LDA and PBE-GGA) and hybrid functionals (HSE03 and PBE0). In figure 4 the d states from these calculations are shown. Using the energy separation between features A and D to quantify the agreement between experiments and theory, we observe a significant improvement when moving from the traditional functionals to the hybrid functionals, see table 3. While the experimentally observed separation between features A and D

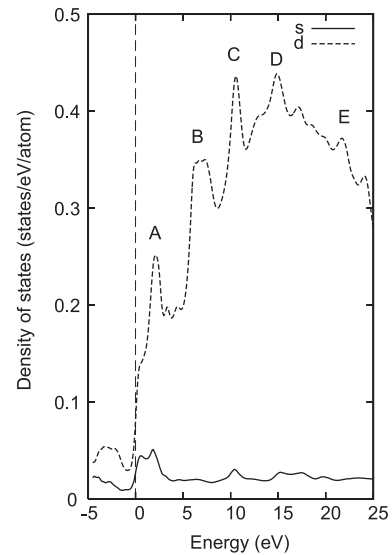


Figure 3. The s and d symmetry projected local DOS of a phosphorus atom with a statically screened hole in the 2p shell. The calculations were performed using the RSMS method.

is larger than all the calculated values, the separation increases by 0.95 eV when going from PBE-GGA to PBE0. Compared to the RSMS calculations the improvement is 1.5 eV. Although this is a clear improvement, the discrepancy is still as much as 13% when comparing the PBE0 calculations with the experimental results. This is caused by the failure to describe the long-range correlation interaction or the lack of exciton effects. To further investigate this, calculations with a corrected correlation interaction are needed.

3.3. Valence band DOS and the bandgap

In the previous section we showed that the description of the conduction band was improved by the use of hybrid

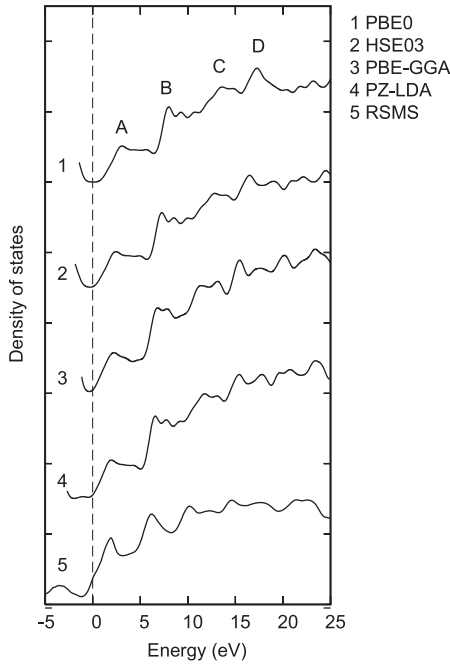


Figure 4. The phosphorus d states calculated using PZ-LDA, PBE-GGA, HSE03 and PBE0 functionals in the framework of DFT. A Gaussian broadening with $\sigma = 0.4$ has been applied to the results. Both a rigid shift (change in bandgap) and an increased dispersion are observed. The ground state d-DOS calculated by the RSMS method is also shown.

Table 3. Separation of features A and D in the calculated DOS using RSMS and DFT, together with the experimental value. The experimental value was found by Gaussian peak fitting to the experimental data.

	$E_D - E_A$ (eV)	Deviation from experiment
RSMS	12.66	-22.5%
PZ-LDA	13.46	-17.6%
PBE-GGA	13.24	-18.9%
HSE03	14.09	-13.7%
PBE0	14.19	-13.1%
Experiments	16.33	—

functionals. We now move on to investigate the bandgap and valence band properties.

Figure 5 shows the ground state DOS calculated using DFT for the PZ-LDA, PBE-GGA, HSE03 and PBE0 functionals. In agreement with previous results [15], the region from the Fermi level to approximately -7 eV is dominated by states with 3p character, while below -12 eV 3s states dominate. Between, at approximately -10 and -6 eV, there are sharp peaks in the DOS of hybridized s and p character.

Black phosphorus is reported to be a semiconductor with a narrow bandgap of $E_g^{\text{exp}} = 0.30\text{--}0.35$ eV [31, 14]. The size of this gap has been shown to be very sensitive to pressure, with a decreasing gap as the pressure is increased [31, 14]. Calculations of the band structure using the tight binding method [51] and the self-consistent pseudo-potential method [15] indicated that this behaviour is due to the reduced interlayer spacing at high pressures, giving

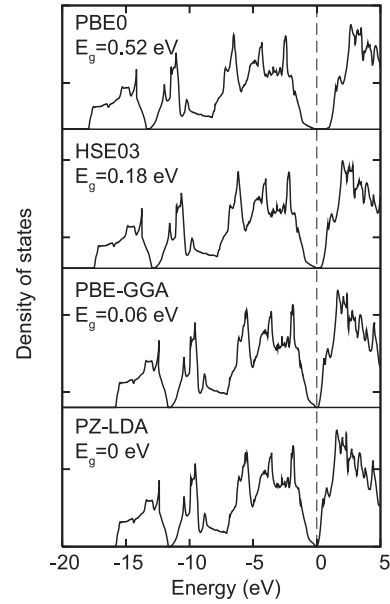


Figure 5. The phosphorus total density of states calculated using the PZ-LDA, PBE-GGA, HSE03 and PBE0 functionals in the framework of DFT. The inclusion of Fock exchange introduces dispersion to the valence states. The predicted bandgap E_g is also indicated.

stronger interlayer interaction and band bending along the Γ -Z direction. Even though the pressure modifies the gap, the major contribution is still expected to originate in a single layer, which is held together by the covalent bonds. Thus, significant differences are expected among the local and semi-local functionals, even though the van der Waals forces are not properly described.

In the PZ-LDA calculations no bandgap is observed, although a narrow region of low DOS is present. The PBE-GGA calculations show a small bandgap $E_g^{\text{PBE}} = 0.08$ eV. For HSE03 the calculated bandgap is $E_g^{\text{HSE03}} = 0.18$ eV, which is 0.12–0.17 eV lower than the experimental values, a correction over the traditional functionals that is known in the literature [52, 53]. Finally, the bandgap predicted from PBE0 is $E_g^{\text{PBE0}} = 0.52$ eV, which is higher than the experimental values by 0.18–0.22 eV. Overestimation of the bandgap is a well-known failure of exact Hartree-Fock calculations and, since PBE0 contains a larger portion of Fock exchange than HSE03, an increased bandgap is expected for PBE0. The difference in bandgap between PBE-GGA and HSE03 is directly related to semi-local delocalization corrections and should then reflect corrections for the covalent layer. However, the difference between HSE03 and PBE0 lies purely in the treatment of long-range exchange. Together with previous studies showing that the bandgap is sensitive to the interlayer interaction [51], the overestimation of the gap in PBE0 indicates a successful exchange residue correction, where most of the artificial van der Waals interaction is removed.

Turning to the valence band, we see that all four approaches shown in figure 5 give similar features in the valence band. However, as with the conduction band, there is a significant increase of dispersion when going from PZ-LDA to PBE0. This effectively yields higher binding energies in the

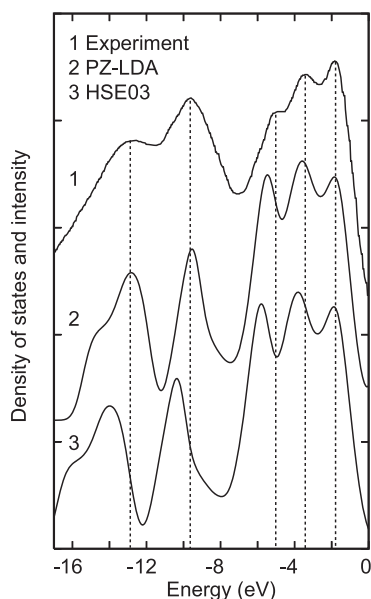


Figure 6. Comparison of the valence band XPS spectrum of phosphorus [30] and the total valence density of states, calculated using the PZ-LDA and HSE03 functionals in the framework of DFT. A Gaussian smearing of $\sigma = 0.4$ has been applied to the results. The added dispersion within HSE03 slightly worsens the experiment's correspondence.

hybrid calculations, a result expected from the delocalization corrections. For example, the s-p hybridized peak which appears in the range -9 to -11 eV in the PZ-LDA calculations, is shifted downwards approximately 1 eV in the PBE0 results.

While the general features are in good agreement with previous work, the increase of dispersion is of concern when comparing to previous experimental investigations of the valence band using x-ray photoelectron spectroscopy (XPS). In figure 6 we compare our calculations to the experiments of Goodman *et al* [30]. While the PZ-LDA calculations show convincing agreement with the experiments, we see that the inclusion of Fock exchange adds a slight dispersion which worsens the agreement with the experiment.

4. Final discussion and conclusions

Perfect agreement between calculations and experiments should not be expected for any of the functionals used here. The hybrid functionals only deal with the inclusion of Fock exchange, while correlation effects are described with the traditional approach of DFT. As a result, the inclusion of long-range Fock exchange in PBE0 causes a significant overestimation of the bandgap, while the dispersion of the conduction band is too small compared to the experimental observations. To obtain better agreement with experiments, proper treatment of the long-range correlation is needed.

In addition, the error cancellation of the PZ-LDA calculations is lifted when the hybrid functionals are introduced. This is caused by the partial delocalization correction, which adds a dispersion to the valence band. Thus, while the PZ-LDA calculations are in good agreement with

the experimental valence band, the inclusion of Fock exchange worsens the correspondence between experiments and theory for the valence band. The HSE03 and PBE0 functionals give an improved correspondence with experiments over the PZ-LDA and PBE-GGA functionals, although mainly in the conduction band.

The isolated covalent layer should include a bandgap [51]. It is thus a welcome result that the HSE03 functional corrects the semi-local delocalization error in the PBE-GGA functional and opens a gap, proving the importance of correcting semi-local errors in structures with both covalent and van der Waals bonding. The PBE0 functional was found not to converge, which we interpret as an indication that the previously proposed [47] partial long-range exchange residue correction remedies parts of the fictitious van der Waals bonding present in the PBE-GGA and HSE03 functionals. This is further strengthened by the overestimation of bandgap under fixed lattice parameters and atom positions.

The agreement between the RSMS calculations and the experimentally obtained EELS spectra was satisfactory in that all features observed experimentally were also present in the calculated spectra. However, there was a significant error in their position in energy, which can be traced back to an inaccurate description of the electronic structure and thus the muffin-tin and local potential method employed in FEFF8.

Acknowledgments

Support from the Norwegian Research Council through the project *Studies of the electronic structure of materials at the nanoscale* is gratefully acknowledged. We would also like to thank O M Løvrvik, J Taftø, S Casolo and J Harl for helpful discussions, and O B Karlsen for sample synthesis.

References

- [1] Hohenberg P and Kohn W 1964 *Phys. Rev.* **136** B864
- [2] Kohn W and Sham L J 1965 *Phys. Rev.* **140** A1133
- [3] Cohen A J, Mori-Sánchez P and Yang W 2008 *Science* **321** 792
- [4] Langreth D C and Mehl M J 1983 *Phys. Rev. B* **28** 1809
- [5] Becke A D 1988 *Phys. Rev. A* **38** 3098
- [6] Perdew J P, Chevary J A, Vosko S H, Jackson K A, Pederson M R, Singh D J and Fiolhais C 1992 *Phys. Rev. B* **46** 6671
- [7] Perdew J P, Chevary J A, Vosko S H, Jackson K A, Pederson M R, Singh D J and Fiolhais C 1993 *Phys. Rev. B* **48** 4978(E)
- [8] Cohen A J, Mori-Sánchez P and Yang W 2008 *Phys. Rev. B* **77** 115123
- [9] Cohen A J, Mori-Sánchez P and Yang W 2008 *J. Chem. Phys.* **129** 121104
- [10] Mori-Sánchez P, Cohen A J and Yang W 2008 *Phys. Rev. Lett.* **100** 146401
- [11] Aryasetiawan F and Gunnarsson O 1998 *Rep. Prog. Phys.* **61** 237
- [12] Cartz L, Srinivasa S R, Riedner R J, Jorgensen J D and Worlton T G 1979 *J. Chem. Phys.* **71** 1718
- [13] Brown A and Rundqvist S 1965 *Acta Crystallogr. A* **19** 684
- [14] Morita A 1986 *Appl. Phys. A* **39** 227
- [15] Asahina H, Shindo K and Morita A 1982 *J. Phys. Soc. Japan* **51** 1193

- [16] Hult E, Rydberg H, Lundqvist B I and Langreth D C 1999 *Phys. Rev. B* **59** 4708
- [17] Harris J 1985 *Phys. Rev. B* **31** 1770
- [18] Heyd J, Scuseria G E and Ernzerhof M 2003 *J. Chem. Phys.* **118** 8207
- [19] Adamo C and Barone V 1999 *J. Chem. Phys.* **110** 6158
- [20] Becke A D 1993 *J. Chem. Phys.* **98** 5648
- [21] Curtis L A, Raghavachari K, Redfern P C and Pople J A 1997 *J. Phys. Chem.* **106** 1063
- [22] Ernzerhof M and Scuseria G E 1999 *J. Chem. Phys.* **110** 5029
- [23] Paier J, Hirschl R, Marsman M and Kresse G 2005 *J. Chem. Phys.* **122** 234102
- [24] Ángyán J G, Gerber I C, Savin A and Toulouse J 2005 *Phys. Rev. A* **72** 012510
- [25] Marsman M, Paier J and Kresse G 2008 *J. Phys.: Condens. Matter* **20** 064201
- [26] Keast V J, Scott A J, Brydson R, Williams D B and Bruley J 2001 *J. Microsc.* **203** 135–75
- [27] Ankudinov A L, Ravel B, Rehr J J and Conradson S D 1998 *Phys. Rev. B* **58** 7565
- [28] Perdew J P and Zunger A 1981 *Phys. Rev. B* **23** 5048
- [29] Perdew J P, Burke K and Ernzerhof M 1996 *Phys. Rev. Lett.* **77** 3865
- [30] Goodman N B, Ley L and Bullett D W 1983 *Phys. Rev. B* **27** 7440
- [31] Keyes R W 1953 *Phys. Rev.* **92** 580
- [32] Lange S, Schmidt P and Nilges T 2007 *Inorg. Chem.* **46** 4028
- [33] Rez P 2004 *Transmission Electron Energy Loss Spectrometry in Materials Science and the EELS Atlas* ed C C Ahn (Weinheim: Wiley) chapter 4, pp 97–126
- [34] Hedin L and Lundqvist B I 1971 *J. Phys. C: Solid State Phys.* **4** 2064
- [35] Ankudinov A L, Nesvizhskii A I and Rehr J J 2003 *Phys. Rev. B* **67** 115120
- [36] Blöchl P E 1994 *Phys. Rev. B* **50** 17953
- [37] Kresse G and Joubert D 1999 *Phys. Rev. B* **59** 1758
- [38] Kresse G and Furthmüller J 1996 *Comput. Mater. Sci.* **6** 15
- [39] Kresse G and Furthmüller J 1996 *Phys. Rev. B* **54** 11169
- [40] Kresse G and Hafner J 1994 *Phys. Rev. B* **49** 14251
- [41] Kresse G and Hafner J 1993 *Phys. Rev. B* **48** 131158
- [42] VASP code <http://cms.mpi.univie.ac.at/vasp>
- [43] Ernzerhof M 1996 *Chem. Phys. Lett.* **263** 499
- [44] Ernzerhof M, Perdew J P and Burke K 1996 *Int. J. Quantum Chem.* **64** 285
- [45] Perdew J P, Ernzerhof M and Burke K 1996 *J. Chem. Phys.* **105** 9982
- [46] Pulay P 1980 *Chem. Phys. Lett.* **73** 393
- [47] Langreth D C, Dion M, Rydberg H, Schröder E, Hyldgaard P and Lundqvist B I 2004 *Int. J. Quantum Chem.* **101** 599
- [48] Weng X, Rez P and Ma H 1989 *Phys. Rev. B* **40** 4175
- [49] Sæterli R, Flage-Larsen E, Prytz Ø, Marthinsen K, Holmestad R and Taftø J 2009 *Phys. Rev. B* **80** 075109
- [50] Prytz Ø, Sæterli R, Løvvik O M and Taftø J 2008 *Micron* **39** 685
- [51] Takao Y, Asahina H and Morito A 1981 *J. Phys. Soc. Japan* **50** 3362
- [52] Heyd J and Scuseria G E 2004 *J. Chem. Phys.* **121** 1187
- [53] Brothers E N, Izmaylov A F, Normand J O, Barone V and Scuseria G E 2008 *J. Chem. Phys.* **129** 011102